NANO LETTERS

pubs.acs.org/NanoLett Letter

Dephasing Dynamics Accessed by High Harmonic Generation: Determination of Electron−Hole Decoherence of Dirac Fermions

Youngjae Kim, Min Jeong Kim, Soonyoung Cha, Shinyoung Choi, Cheol-Joo Kim, B. J. Kim, Moon-Ho Jo, Jonghwan Kim,* and JaeDong Lee*

Cite This: *Nano Lett.* 2024, 24, 1277−1283 Read Online

ACCESS | Metrics & More | Article Recommendations | Supporting Information

ABSTRACT: We reveal the critical effect of ultrashort dephasing on the polarization of high harmonic generation in Dirac fermions. As the elliptically polarized laser pulse falls in or slightly beyond the multiphoton regime, the elliptically polarized high harmonic generation is produced and exhibits a characteristic polarimetry of the polarization ellipse, which is found to depend on the decoherence time T_2. T_2 could then be determined to be a few femtoseconds directly from the experimentally observed polarimetry of high harmonics. This shows a sharp contrast with the semimetal regime of higher pump intensity, where the polarimetry is irrelevant to T_2. An access to the dephasing dynamics would extend the prospect of high harmonic generation into the metrology of a femtosecond dynamic process in the coherent quantum control.

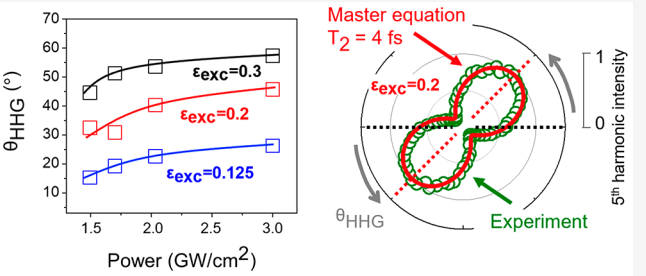

KEYWORDS: *high harmonic generation spectroscopy, graphene, decoherence time, quantum master equation*

Downloaded via POHANG UNIV OF SCIENCE & TECHNOLOGY on April 21, 2024 at 09:27:24 (UTC).
See https://pubs.acs.org/sharingguidelines for options on how to legitimately share published articles.

Over the past decades, laser-driven electron dynamics leading to fascinating nonlinear phenomena behind the deep inside of ultrafast physics have attracted a great deal of attention in condensed matter physics.[1−5] Such dynamics can be decomposed into higher harmonic electron motions deserving radiations, which we call the high harmonic generation (HHG).[6] Beyond the fact that the harmonic generation techniques have been considered useful methods for an ultrafast imaging microscope, the light conversion, and the coherent light source exploration,[7−9] now the most powerful advantage of HHG has become to identify excited dynamics and unveil various information on nonequilibria reaching the petahertz frequency benchmark.[10−12]

Since the condensed matter consists of periodically ordered atomic arrangements and orbital hybridizations, the resulting HHG accompanies a variety of emission processes incorporated with distinct quantum pathways of excited electrons.[13−22] Recently, under the elliptically polarized pump pulse, a number of studies have revealed the substantial ellipticity dependence of HHG across a wide range of materials from graphene[5] to surface states of topological insulators,[23,24] in addition to typical semiconductors,[25] reflecting the unique electron dynamics inherent to those characteristic electronic structures. In graphene, as a representative Dirac material, the fifth- and seventh-order harmonic generations are found to show an enhanced intensity under the elliptically polarized laser with a strong light wave, which would be due to the strong semimetalization nature of the Dirac band structure.[5] In a microscopic respect, such an increase of the HHG signal is attributed to the nonlinear couplings between interband and intraband transitions.[26] With these findings, the scope of HHG has been significantly widened to explore novel quantum-mechanical perspectives in various Dirac systems.[27]

While the interplays between distinct transition channels provide unique harmonic sources, the decoherence now can interfere with the release of HHG depending on the scattering nature.[28−36] The decoherence time T_2, i.e., the dephasing time for loss of electron−hole coherence due to the coupling with nonequilibrium dissipation, is of utmost importance for the physics of coherent quantum control, for instance, like quantum information and computing.[37,38] In contrast to the population decay T_1,[39] the measurement of T_2 usually requires highly nontrivial methods,[40] including the four-wave mixing[41] and pump−probe technique,[42] which just remain in the limited and relative time scale. Beyond the pump−probe scheme, it would be timely to suggest an exquisite pathway for an estimation of T_2 on the basis of quantified evidence for the scattering nature, resulting in the dissipation and the relevant dynamic links among underlying physics.

Received: November 6, 2023
Revised: January 10, 2024
Accepted: January 11, 2024
Published: January 17, 2024

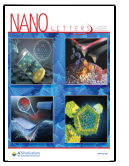

ACS Publications © 2024 American Chemical Society

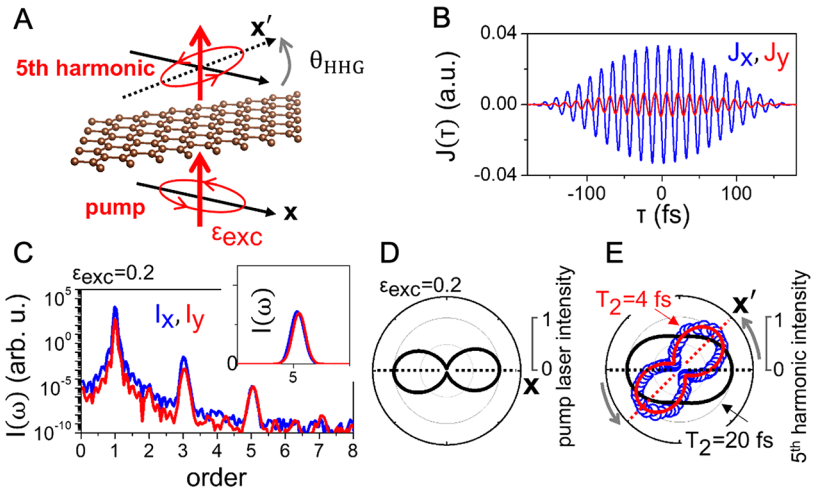

Figure 1. Fifth-order harmonic generations in graphene. (A), The fifth-order harmonic generation released undergoes a rotation of the major axis of the polarization ellipse by an angle of θ_{HHG} (an angle between the major axis of pump laser, i.e. $\hat{\boldsymbol{x}}$ and the rotated major axis of the fifth-order harmonic, i.e. $\hat{\boldsymbol{x}}'$). (B) Calculation of the time-dependent current densities, $\boldsymbol{J}(\tau)$ under the pump pulse with $\varepsilon_{exc} = 0.2$, $\omega_0 = 0.275$ eV, and $E_0 = 8.5$ mV/Å. (C) HHG spectra calculated from $\boldsymbol{J}(\tau)$. The inset gives an enlargement of the fifth-order harmonic in the linear scale. The ratio of fifth-order intensities I_y/I_x clearly exceeds a given ellipticity of the pump pulse field, which implies that the polarization direction where the fifth-order harmonic is maximally emitted should be rotated with respect to the $\hat{\boldsymbol{x}}$-direction. (D) Polar plot of the normalized pump intensity. (E) T_2-dependent polar plots of the normalized fifth-order harmonics. Blue circles represent the experimental results.

In this paper, we make theoretical and experimental investigations of the ultrafast decoherence of graphene focusing on the fifth-order harmonic generation under the elliptically polarized laser pump, where the harmonic emission is also elliptically polarized and shows a unique polarimetry of the polarization ellipse. When elliptically polarized pumping is attempted within or slightly beyond the multiphoton regime, the intraband channels gradually contribute along with the already strong interband channels. Then, polarimetry such as the rotation angle and the ellipticity of the polarization ellipse is found to be highly sensitive to the decoherence time T_2, which enables a quantitative determination of T_2 from the experiment and is eventually revealed to be a few femtoseconds. In sharp contrast, in the semimetal regime of higher pump laser intensity, the interband channels become minorities, and a rotation of the polarization ellipse of HHG is irrelevant to T_2 for 2 fs $\leq T_2 \leq$ 50 fs. Our understanding of the dynamic linking among quantum pathways which underlies HHG will give a new route to achieve the metrology of femtosecond dephasing dynamics beyond the conventional reach of HHG.

Rotation of Polarization Ellipse of HHG. To investigate the real-time dynamics of the fifth-order harmonic generation, we employ the quantum master equation[26] with the light-wave interacting Dirac Hamiltonian expanded from momenta $\mathbf{K}$ and $-\mathbf{K}$, which reads $\partial/\partial\tau\rho_{\mathbf{k}}(\tau) = -i/\hbar[H_{\mathbf{k}(\tau)},\rho_{\mathbf{k}}(\tau)] + \hat{S}[\rho_{\mathbf{k}}(\tau)]$, where $\rho_{\mathbf{k}}(\tau)$ is the density matrix in the Houston basis describing the electronic states at the momentum $\mathbf{k}(\tau)$. The Hamiltonian $H_{\mathbf{k}(\tau)}$ evolves the light−matter interaction under a pump laser with a peak electric field strength of E_0, a frequency of ω_0, and an ellipticity of ε_{exc} (Figures S3 and S4). When the reflection loss and dielectric environment of the ion-gel generating local-field effects in the experiment are considered, the dielectric screened field strength of 8.5 mV/Å for E_0 is taken and the corresponding Rabi frequency ω_R turns out to be $\sim 0.75\omega_0$, which is a bit above the criterion of the multiphoton regime ($\sim 0.5\omega_0$).[34] Here the intraband channels somewhat contribute to the strong interband channels. This shows a good agreement with the peak intensity of the experimental laser source of 3 GW/cm^2 in a vacuum (Figures S1 and S2). Solving the quantum master equation, the current density could be evaluated as $\boldsymbol{J}(\tau) = \sum_{\mathbf{k}}\rho_{\mathbf{k}}\ \mathrm{Tr}[\partial H_{\mathbf{k}(\tau)}/\partial\mathbf{k}\rho_{\mathbf{k}}(\tau)]$ and the HHG spectrum as $I(\omega) \approx \omega^2|\boldsymbol{J}(\omega)|^2$ with $\boldsymbol{J}(\omega) = \int d\tau\, \boldsymbol{J}(\tau)e^{i\omega\tau}$. The spectral weight is then defined to be $I^{nth} = \int_{(n-1/2)\omega_0}^{(n+1/2)\omega_0} d\omega\ I(\omega)$ for the nth-order harmonic. For the dephasing term, we define $[\rho_{\mathbf{k}}(\tau)]_{\mu\nu} = -(1-\delta_{\mu\nu})\rho_{\mathbf{k}}^{\mu\nu}(\tau)/T_2$, where μ and ν are band indices, and then consider the interband electron−hole coherence with the characteristic decoherence time T_2.[26] We do not include the relaxation processes microscopically, but the dephasing time T_2 of $\langle c_{\mathbf{k}}^{\dagger}d_{\mathbf{k}}^{\dagger}\rangle$ or $\langle d_{\mathbf{k}}c_{\mathbf{k}}\rangle$[32,33] with electron ($c_{\mathbf{k}}^{\dagger}$ or $c_{\mathbf{k}}$) and hole operators ($d_{\mathbf{k}}^{\dagger}$ or $d_{\mathbf{k}}$). Considering the excitation intensity adopted in this study, the decoherence time is an essential factor in the HHG emission. Therefore, we ignore the population decay T_1, i.e., numerically $T_1 \gg T_2$, which would not affect the dynamics much (Figure S7). It is notable that, in contrast to the fifth-harmonic emission, the third-harmonic emission is found to exhibit less polarimetry dependence due to its weaker nonlinearity (Figure S8).

As shown in the schematic of Figure 1A, the polarization ellipse of the fifth-order harmonic undergoes a rotation angle of θ_{HHG} with respect to the pump pulse. In Figure 1B, the time-dependent current densities are provided along the $\hat{\boldsymbol{x}}$- and -directions for a given ellipticity of the pump laser ($\varepsilon_{exc} = 0.2$). As can be seen, the amplitude of the current along the -direction is larger than that along the -direction. Figure 1C displays the HHG spectra obtained from the time-dependent current densities of Figure 1B. I_x of the third-order harmonic is observed to be clearly larger than I_y, whereas in the fifth-order harmonics I_x and I_y are almost comparable to each other. In Figure 1D, the polar plot of the pump pulse intensity is shown with $\varepsilon_{exc} = 0.2$ whose major axis is aligned along the -direction. Polar plots of the resulting fifth-order harmonic spectra are depicted in Figure 1E for two different values of T_2. It is worth noting that the polarization ellipse of HHG with $T_2 = 4$ fs is rotated by an angle of θ_{HHG} ($\sim 45°$), which is in excellent agreement with the experiment (blue circles). However, a

https://doi.org/10.1021/acs.nanolett.3c04278
Nano Lett. 2024, 24, 1277−1283

longer T_2 (=20 fs) suppresses the rotation, which is obviously not consistent with the experiment. This provides critical evidence that, in the relevant pump intensity, θ_{HHG} should be governed by T_2, implying the possibility to determine T_2 from quantitative measurements of θ_{HHG} from the corresponding experiments.

The rotation of the polarization ellipse of the fifth-order harmonic generation is illustrated as a function of T_2 in Figure 2A. At T_2 longer than T_{pump}, the polarization ellipse is hardly

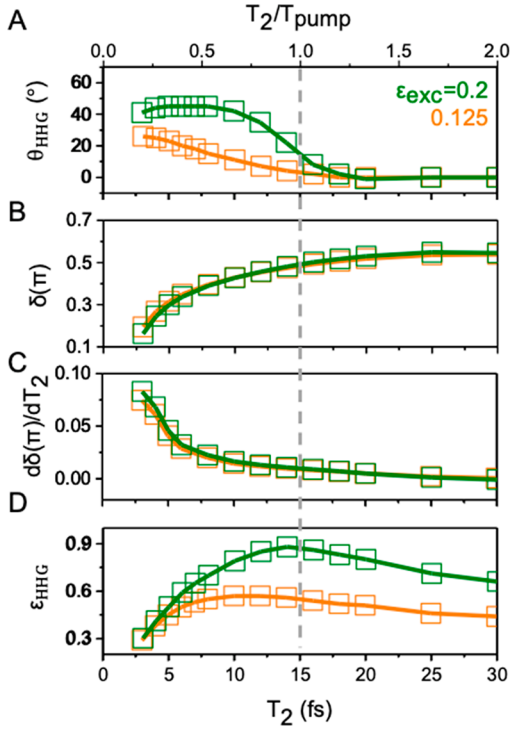

Figure 2. Polarimetry of the theoretical fifth-order harmonic emission. (A) Rotation angle θ_{HHG} of the fifth-order harmonic with respect to T_2 at ε_{exc} = 0.125 and 0.2. (B) Phase difference δ between the two perpendicular current densities, i.e., $\delta = \mathrm{Arg}[J_x(5\omega_0)/J_y(5\omega_0)]$ with respect to T_2. (C) T_2 derivative of the phase difference δ. (D) Ellipticity of the fifth-order harmonic. T_{pump} is a single period of the pump oscillation, $T_{pump} = 2\pi/\omega_0$ = 15 fs (i.e., ω_0 = 0.275 eV).

rotated and is found to coincide with that of the pump pulse. In contrast, the polarization ellipse now starts to rotate as T_2 becomes shorter than T_{pump} and gets to be maximized at a few femtoseconds of T_2. This would be interpreted from the phase difference of δ between $J_x(5\omega_0)$ and $J_y(5\omega_0)$. In Figure 2B, at T_2 longer than T_{pump}, the δ reaches $\sim\pi/2$, indicating $\theta_{HHG} \approx 0°$ whereas, at T_2 shorter than T_{pump}, δ gradually drops and indicates a finite rotation of θ_{HHG}. Further, in Figure 2C, the derivative of δ, i.e., $d\delta/dT_2$, is displayed, which delivers a message that the attained phase delay for δ would be related to T_2 accompanying the relative time scale of T_{pump}. Additionally, in Figure 2D, ε_{HHG}, the ellipticity of the fifth-order harmonic emission, also shows the T_2-dependence. At $T_2 \lesssim T_{pump}$, the intraband channels are fairly considerable compared to the interband channels (the intraband acceleration process is scaled by the pump duration, i.e., T_{pump}), where the intraband channels perpendicular to the major axis of the polarization play a role in developing the polarimetry such as θ_{HHG} and ε_{HHG}. On the other hand, at $T_2 \gg T_{pump}$, the contribution from persistent interband channels gets to be dominant and that from intraband ones perpendicular to the major axis of the polarization is rather suppressed. This would make an observation of the polarimetry diminish over $\sim T_2$.

Determination of Absolute Value T_2 under a Specific HHG Condition. Based on the rotation of the polarization ellipse in the fifth-order harmonic emission, we can determine T_2 by making a connection between theory and experiment. In Figure 3A, experimental results of the sublaser-cycle HHG spectroscopy are provided between the pump laser intensity and ellipticity (ε_{exc} = 0.125, 0.2, and 0.3) and the rotation angle θ_{HHG}. For experimental data points in the dashed gray box, from the theoretical curve of θ_{HHG} with respect to T_2 for a given pump intensity (i.e., for 3 GW/cm^2) in Figure 3B, we could determine values of T_2 of graphene (black arrows) to reproduce experimental observations of θ_{HHG}. In particular, for ε_{HHG} = 0.2, out of α and β on a broad peak of θ_{HHG} at 4 fs $\lesssim T_2 \lesssim$ 8 fs, α could be set to a true T_2 by an additional consideration of ε_{HHG} (see the inset). That is, as implied from the theoretical curve of ε_{HHG} with respect to T_2 (Figure 2D), we could also determine T_2 from experimental observations of ε_{HHG}. When the intensity increases to 3 GW/cm^2, as shown in Figure 3C, observations of both θ_{HHG} (solid line) and ε_{HHG} (dashed line) result in effectively the same value (i.e., a single value) of T_2. That is, the two sets of lines converge, leading to a well-defined T_2. On the other hand, under the weak pump intensities of 1.5−2 GW/cm^2, observations of θ_{HHG} and ε_{HHG} are found to give somewhat scattered values of T_2. That is, the shaded areas are determined to be ones enclosed by solid and dashed lines, implying scattered values of T_2. This is largely due to polar deviations of the experimental data of weak pump sectors, especially in ε_{HHG} (see the inset), which lead to unavoidable ambiguities. In the high-power regime, the experimental polar spectra nicely agree with the theoretical fit lines, corresponding to a minimal error deviation as $\bar{d}$ localizes near $\Delta I \approx 0$. In the low-power regime, however, $\bar{d}$ displays a more dispersed distribution, which hinders an accurate determination of T_2. In this sense, determinations of T_2 through ε_{HHG} are supplemented as lower bounds of T_2 in Figure 3C. Surprisingly, to reach the experimental observation of θ_{HHG} for given values of ε_{HHG} at the intensity of 3 GW/cm^2, T_2 should be 3−4 fs, much shorter than ~20 fs widely taken in previous studies.[26,35,36] It is noticeable that T_2 is found to converge to 3−4 fs in a range of ε_{exc} = 0.12−0.5 (Figure S16). A complete process of electron−hole creation and recombination requires the coherence of an electron−hole pair so that this process should be scaled by the decoherence time T_2.[43] Along the line, the decoherence time of a few fs to reproduce the HHG of graphene of the present study may be understood. The fast group velocity of Dirac fermions leads to a substantially large separation between electron and hole just after the interband transition in graphene, which would make the probability of recombination drastically suppressed and thus the decoherence time T_2 to be only a few femtoseconds. Furthermore, we give the HHG characteristic curve of graphene to describe the linked correlation between T_2 and θ_{HHG} for the pump intensity and ellipticity in Figure 3D. The pump pulse with a sizable ellipticity would cause the number of charged carriers in the metallic sectors of the Dirac cone, which instantaneously enhances the dielectric screening between excited electrons and holes and eventually makes an increase of T_2 (Figures S9 and S10 and ref 46).

Phase Relations. The phase difference δ of Figure 2B can be actually suggestive of the anisotropy due to the rotation of

https://doi.org/10.1021/acs.nanolett.3c04278
Nano Lett. 2024, 24, 1277−1283

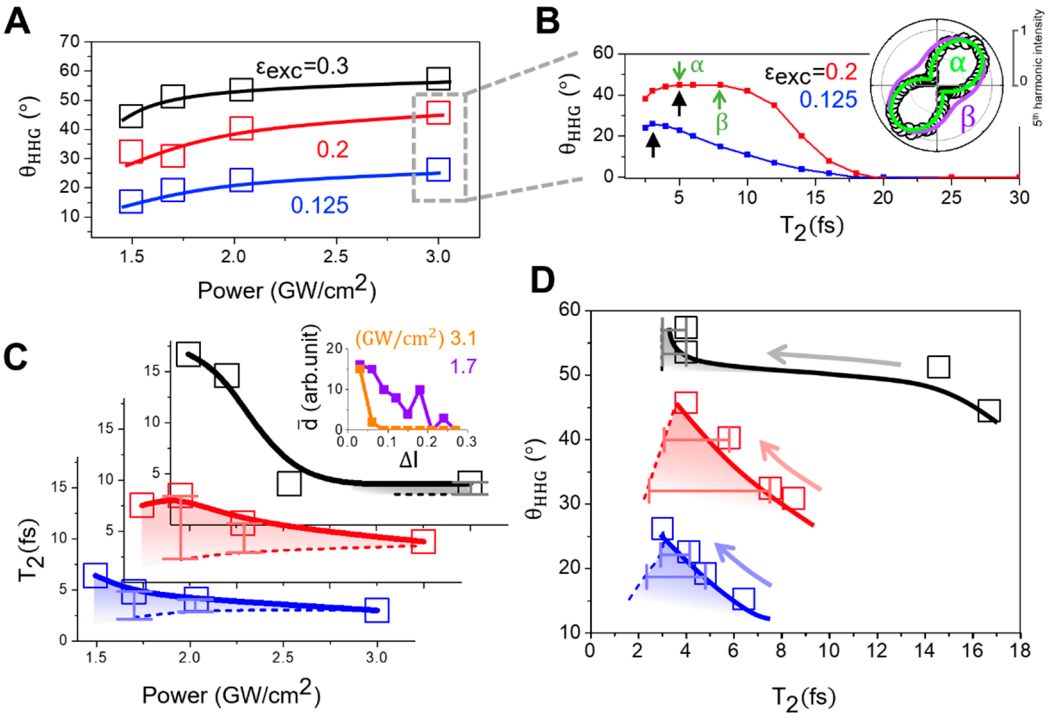

Figure 3. Determination of T_2 and linked correlation. (A) Experimental results of θ_{HHG} with respect to the laser intensity at a few values of ε_{exc} from the ultrafast high harmonic spectroscopy (Figures S3 and S4). (B) For points in the gray dashed box of (A), theoretical calculations of θ_{HHG} are given with respect to T_2. Black arrows point out determined values of T_2. The inset shows the theory with α (green line) and β (purple line) and the experiment (black circle) for $\varepsilon_{exc} = 0.2$. (C) T_2 determined from experiments with respect to the pump intensity. Solid lines are determined by comparing θ_{HHG} between theoretical and experimental results, whereas dashed lines are based on ε_{HHG}. The two sets of lines are so converged as to lead to an accurate determination of T_2 in 3.1 GW/cm^2. In the inset, polar deviations for 3.1 and 1.7 GW/cm^2 are displayed at $\varepsilon_{exc} = 0.2$, i.e., $\bar{d}(\Delta I) = \frac{1}{2\pi}\int_0^{2\pi} d\theta\, \delta(\bar{\eta}(\theta) - \Delta I)$ with $\bar{\eta}(\theta) = \sqrt{I_{exp}(\theta)^2 - I_{fit}(\theta)^2}$. ΔI indicates the standard deviation of the experimental fifth-harmonic intensity $I_{exp}(\theta)$ (Figure S13). (D) HHG characteristic curve between T_2 and θ_{HHG} for the pump intensity and ellipticity. Arrows indicate directions to increase the pump intensity. (C, D) Solid lines and dotted lines indicate determinations of T_2 based on the experimental observations of θ_{HHG} and ε_{HHG} (not so much available for $\varepsilon_{exc} = 0.3$), respectively. In (A), (C), and (D), blue, red, and black denote cases with $\varepsilon_{exc} = 0.125$, 0.2, and 0.3, respectively. A similar interplay between the degree of coherence and the induced many-body interaction has been also reported in a previous study,[42] where the modified many-body interaction due to the number of excited carriers enables estimation of a relative change in T_2 compared to a reference experiment. In contrast, the determination of T_2 in our study should be regarded as absolute dephasing dynamics accessed by HHG under a specific optical condition, since it can be directly quantified through the polarimetry observations for the high harmonic emission.

the polarization ellipse; at $T_2 > T_{pump}$, $J(\theta,5\omega_0)$ is reduced to cos $\theta|J_x(5\omega_0)| + i$ sin $\theta|J_y(5\omega_0)|$ and gets to be more or less isotropic for instance at $\theta \leq \pm 40°$, whereas at $T_2 \ll T_{pump}$, $J(\theta,5\omega_0)$ is reduced to cos $\theta|J_x(5\omega_0)| +$ sin $\theta|J_y(5\omega_0)|$ and becomes substantially anisotropic. For an in-depth understanding of the dynamics, however, explicit quantum pathways could be taken into account. The fifth-order harmonic yields can be obtained from the current density as a sum of interband and intraband channel contributions, i.e., $\boldsymbol{J}(5\omega_0) = \boldsymbol{J}_{inter}(5\omega_0) + \boldsymbol{J}_{intra}(5\omega_0)$, which eventually produces the HHG spectrum $I(5\omega_0)$. $\boldsymbol{J}_{inter}(\tau) = \sum_{\mathbf{k}} \mathrm{Tr}[\partial H_{\mathbf{k}(\tau)}/\partial\, \mathbf{k}\rho_{\mathbf{k}}^{(off\text{-}diag)}(\tau)]$ and $\boldsymbol{J}_{inter}(\tau) = \sum_{\mathbf{k}} \mathrm{Tr}[\partial H_{\mathbf{k}(\tau)}/\partial\, \mathbf{k}\rho_{\mathbf{k}}^{(diag)}(\tau)]$ can be given by decomposing the density matrix $\rho_{\mathbf{k}}(\tau)$ into ones involving only off-diagonal and diagonal elements. Further, we introduce the θ-dependent current density from $J_{inter/intra}(\theta,\tau) = \cos\theta\, J_{inter/intra;x}(\tau) + \sin\theta\, J_{inter/intra;y}(\tau)$. Now the phase difference $\phi(\theta)$ between $J_{inter}(\theta,5\omega_0)$ and $J_{intra}(\theta,5\omega_0)$ would govern the interference between interband and intraband channels, which would be important not only for the harmonic intensity itself but also for the rotation of the polarization ellipse. The phase of $0 < \phi(\theta) < \pi/2$ signifies that interband and intraband channels should be constructive, whereas the phase of $\pi/2 < \phi(\theta) < \pi$ signifies that the two channels are destructive. According to Figure 4A,B, the fifth-order harmonic is found to be produced entirely through the destructive interference. When $T_2 > T_{pump}$ (Figure 4A), the phase difference $\phi(\theta)$ looks rather isotropic with respect to the polarization angle θ and the polarization of HHG coincides with that of the pump pulse. However, when $T_2 \ll T_{pump}$ (Figure 4B), $\phi(\theta)$ has anisotropic θ dependences, that is, more destructive along $\sim -45°$ but less destructive along $\sim +45°$. In this case, such a rapid dissipation for interband channels before a complete rotation of the elliptically polarized pulse driving intraband channels mainly results in anisotropic interference, which clearly supports the rotation of the polarization ellipse and phase δ consistently with Figure 2A,B.

Emission Rule for Harmonic Generation. Finally, we discuss the underlying physics as to how dynamics of the fifth-order harmonic generation is connected to the decoherence and the laser intensity from the 3 G W/cm^2 to the semimetal regime (i.e., higher pump intensity $\sim$0.8 TW/cm^2).[5] In the semimetal regime ($\omega_R \gg 1.5\omega_0$) of Figure 4C (also see its inset), the rotation of the polarization ellipse is found to be irrelevant to T_2 for 2 fs $\leq T_2 \leq$ 50 fs, which is consistent with the previous theoretical report that the ellipsometry modulation is less pronounced in the decoherence time.[44] The

https://doi.org/10.1021/acs.nanolett.3c04278
Nano Lett. 2024, 24, 1277−1283

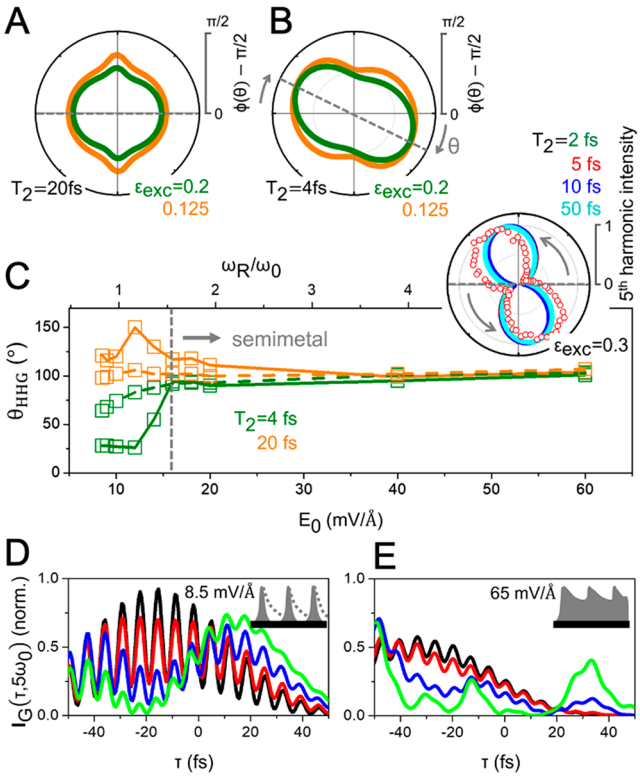

Figure 4. Phase relation and emission rule. (A, B), Polar plots of the phase difference $\phi(\theta)$ (in fact, $\phi(\theta) - \pi/2$) between interband and intraband channels, i.e., $\phi(\theta) = \mathrm{Arg}[J_{\mathrm{inter}}(\theta,5\omega_0)/J_{\mathrm{intra}}(\theta,5\omega_0)]$ for T_2= 20 and 4 fs. (C) Entering the semimetal regime with $\omega_R \geq 1.5\omega_0$ at $\varepsilon_{\mathrm{exc}}$ = 0.2 (solid line) and 0.3 (dashed line), the rotation angle θ_{HHG} gets to be irrelevant to T_2. Here a pulse duration with $2\tau_0$ = 150 fs is adopted, which is shorter than our experimental case. In the inset, the polar plot of the normalized fifth-order harmonics under higher pump field strength with E_0 = 65 mV/Å belonging to the semimetal regime, where red circles denote the experimental observation.[5] Reproduced or adapted with permission from ref 5. Copyright 2023 the American Association for the Advancement of Science. (D, E), Gabor transformations and the emission rule (insets). $I_G(\tau,\omega)$ is normalized from $(s_G\omega/\sqrt{2\pi}) \int d\tau' I_x(\tau')e^{i\omega\tau'}e^{-0.5(\tau'-\tau)^2(s_G\omega)^2}$ for the emission along the major axis in multiphoton and semimetal regimes at $\varepsilon_{\mathrm{exc}}$ = 0.2. s_G = 0.65 is taken. Black, red, blue, and green lines denote T_2 values of 4, 10, 20, and 40 fs, respectively. In addition, our theoretical investigation suggests that the polarimetry dependence is robust not only in massless Dirac systems but also in massive ones. This finding could provide more generalized insights into the polarimetry dependence beyond the scope of massless Dirac systems (Figure S12).

harmonic generation in this regime would vary mostly depending on the Rabi frequency induced from the strong optical field so that the interband channels rarely contribute to the HHG emission. This means that usual assumptions of $T_2 \approx$ 20 fs for understanding the experimental HHG spectra in the semimetal regime is hardly justified, as displayed in Figure 4C. Moreover, our theory in this regime almost reproduces the experimental results of the fifth-order HHG[5] indicated by red bubbles (see the inset) regardless of the decoherence time. In contrast to the semimetal regime, in the multiphoton regime of $\omega_R \ll 1.5\omega_0$, the decoherence expressed by T_2 becomes an essential parameter for the harmonic generation mechanism and the resultant polarimetry. An important difference between the multiphoton and semimetal regimes may be the temporal interference involved in the harmonic emission in the time domain. In the multiphoton regime of Figure 4D, according to the emission rule (see the inset of Figure 4D) for HHG to emit in each half period ($T_{\mathrm{pump}}/2$) of the incident field,[34] the temporal interference and the decoherence would determine the temporal emission train of HHG in a detailed fashion. Thus, the fifth-harmonic emissions and their polarimetry should significantly depend on T_2 especially when $T_2 \lesssim T_{\mathrm{pump}}$. In the semimetal regime of Figure 4E, however, the emission rule is perpetually broken due to the overwhelming interfering overlap between field-driven modified upper and lower Dirac bands, which inhibits the decoherence from playing a role in harmonic generation. Hence, the HHG emissions in this regime are found to have T_2-irrelevant large continuum backgrounds compared to well-defined sharp emission peaks in Figure 4D. Consequently, in the regime, the harmonic generation process becomes irrelevant to T_2 (Figure S11). Meanwhile, in both regimes, at $T_2 \gg T_{\mathrm{pump}}$, severe temporal interferences among enduring polarizations strengthen the T_2 irrelevance. Eventually, the emission rule is claimed to be well satisfied only in the regime of $\omega_R \ll 1.5\omega_0$, that is, under E_0 = 8.5 mV/Å. In particular, we note that in this regime $T_2 \lesssim T_{\mathrm{pump}}$ is the very one which can determine the decoherence time on the basis of HHG experimental investigations. Furthermore, under a consideration of classical recollision processes for HHG of graphene, we could relate the harmonic ellipticity to the decoherence time. This suggests that harmonic processes involving such short recollision distances are essential for achieving the measurable ellipsometry, which is insightfully consistent with the semiclassical approach to predict the minimum recollison distance.[47]

When Dirac electrons are excited by the elliptically polarized laser pulse, the elliptically polarized HHG is produced and undergoes rotation of its polarization ellipse. The relation between the decoherence time T_2 and the polarimetry, especially θ_{HHG}, of the polarization ellipse has been explored. As the elliptically polarized pulse falls in or slightly beyond the multiphoton regime, the polarimetry of fifth-harmonic emission enables determination of T_2. From the experimental observation of θ_{HHG}, we could have determined T_2 belonging to a few femtoseconds in this regime of graphene. This finding is contrasted with the semimetal regime for higher laser intensity, where the rotation of the polarization ellipse is irrelevant to T_2. Understanding and determining the electron−hole decoherence with HHG in high complexities will open novel opportunities to access nonequilibrium dynamics of various electronic processes, including quantum information applications[37,38] and the petahertz electronics.[45]

■ ASSOCIATED CONTENT

Supporting Information

The Supporting Information is available free of charge at https://pubs.acs.org/doi/10.1021/acs.nanolett.3c04278.

Experiment of HHG, device fabrication, infrared transmission spectroscopy, HHG measurements, representation of the Houston basis, comparison between theoretical and experimental results and determination of T_2, and theoretical demonstration of high harmonic emissions (PDF)

https://doi.org/10.1021/acs.nanolett.3c04278
Nano Lett. 2024, 24, 1277−1283

AUTHOR INFORMATION

Corresponding Authors

JaeDong Lee − *Department of Physics and Chemistry, DGIST, Daegu 42988, Republic of Korea*; Email: jdlee@dgist.ac.kr

Jonghwan Kim − *Department of Materials Science and Engineering, POSTECH, Pohang 37673, Republic of Korea; Center for Epitaxial van der Waals Quantum Solids, Institute for Basic Science (IBS), Pohang 37673, Republic of Korea*; Email: jonghwankim@postech.ac.kr

Authors

Youngjae Kim − *Department of Physics and Chemistry, DGIST, Daegu 42988, Republic of Korea; School of Physics, KIAS, Seoul 02455, Republic of Korea*; orcid.org/0000-0002-4544-2940

Min Jeong Kim − *Department of Materials Science and Engineering, POSTECH, Pohang 37673, Republic of Korea; Center for Epitaxial van der Waals Quantum Solids, Institute for Basic Science (IBS), Pohang 37673, Republic of Korea*

Soonyoung Cha − *Center for Epitaxial van der Waals Quantum Solids, Institute for Basic Science (IBS), Pohang 37673, Republic of Korea*

Shinyoung Choi − *Center for Epitaxial van der Waals Quantum Solids, Institute for Basic Science (IBS), Pohang 37673, Republic of Korea; Department of Chemical Engineering, POSTECH, Pohang 37673, Republic of Korea*; orcid.org/0000-0001-5465-7719

Cheol-Joo Kim − *Center for Epitaxial van der Waals Quantum Solids, Institute for Basic Science (IBS), Pohang 37673, Republic of Korea; Department of Chemical Engineering, POSTECH, Pohang 37673, Republic of Korea*; orcid.org/0000-0002-4312-3866

B. J. Kim − *Department of Physics, POSTECH, Pohang 37673, Republic of Korea; Center for Artificial Low Dimensional Electronic Systems, Institute for Basic Science (IBS), Pohang 37673, Republic of Korea*

Moon-Ho Jo − *Department of Materials Science and Engineering, POSTECH, Pohang 37673, Republic of Korea; Center for Epitaxial van der Waals Quantum Solids, Institute for Basic Science (IBS), Pohang 37673, Republic of Korea*; orcid.org/0000-0002-3160-358X

Complete contact information is available at: https://pubs.acs.org/10.1021/acs.nanolett.3c04278

Author Contributions

Y.K. and J.L. materialized the study and wrote the paper. Y.K. carried out the numerical work. J.K. led the experiment with M.J.K., S. Cha, S. Choi, C.-J.K., B.J.K., and M.-H.J.. All of authors discussed the results together.

Notes

The authors declare no competing financial interest.

ACKNOWLEDGMENTS

This work was supported by the Basic Science Research Program (2022R1A2B5B01001582) through the National Research Foundation of Korea (NRF), funded by the Ministry of Science and ICT. Y.K. and J.D.L. acknowledge the partial support of computational resources by the Center for Advanced Computation (CAC) at the Korea Institute for Advanced Study (KIAS). J.K. and M.J.K. acknowledge the support from the National Research Foundation of Korea (NRF-2020R1A4A1018935, and 2020R1A2C2103166). J.K. also acknowledges the support from the Institute for Basic Science (IBS) under Project Code IBS-R034-D1.

REFERENCES

(1) Corkum, P. B.; Krausz, F. Attosecond science. *Nat. Phys.* **2007**, *3*, 381−387.

(2) Krausz, F.; Ivanov, M. Attosecond physics. *Rev. Mod. Phys.* **2009**, *81*, 163.

(3) Schubert, O.; Hohenleutner, M.; Langer, F.; Urbanek, B.; Lange, C.; Huttner, U.; Golde, D.; Meier, T.; Kira, M.; Koch, S. W.; Huber, R. Sub-cycle control of terahertz high-harmonic generation by dynamical Bloch oscillations. *Nat. Phys.* **2014**, *8*, 119−123.

(4) Langer, F.; Hohenleutner, M.; Schmid, C. P.; Poellmann, C.; Nagler, P.; Korn, T.; Schüller, C.; Sherwin, M. S.; Huttner, U.; Steiner, J. T.; Koch, S. W.; Kira, M.; Huber, R. Lightwave-driven quasiparticle collisions on a subcycle timescale. *Nature* **2016**, *533*, 225−229.

(5) Yoshikawa, N.; Tamaya, T.; Tanaka, K. High-harmonic generation in graphene enhanced by elliptically polarized light excitation. *Science* **2017**, *356*, 736−738.

(6) Golde, D.; Meier, T.; Koch, S. W. High harmonics generated in semiconductor nanostructures by the coupled dynamics of optical inter- and intraband excitations. *Phys. Rev. B* **2008**, *77*, 075330.

(7) Malard, L. M.; Alencar, T. V.; Barboza, A. P. M.; Mak, K. F.; de Paula, A. M. Observation of intense second harmonic generation from MoS_2 atomic crystals. *Phys. Rev. B* **2013**, *87*, No. 201401(R).

(8) Li, D.; Xiong, W.; Jiang, L.; Xiao, Z.; Rabiee Golgir, H.; Wang, M.; Huang, X.; Zhou, Y.; Lin, Z.; Song, J.; Ducharme, S.; Jiang, L.; Silvain, J.-F.; Lu, Y. Multimodal nonlinear optical imaging of MoS_2 and MoS_2-based van der Waals heterostructures. *ACS Nano* **2016**, *10*, 3766−3775.

(9) Yao, K.; Yanev, E.; Chuang, H.-J.; Rosenberger, M. R.; Xu, X.; Darlington, T.; McCreary, K. M.; Hanbicki, A. T.; Watanabe, K.; Taniguchi, T.; Jonker, B. T.; Zhu, X.; Basov, D. N.; Hone, J. C.; Schuck, P. J. Continuous wave sum frequency generation and imaging of monolayer and heterobilayer two-dimensional semiconductors. *ACS Nano* **2020**, *14*, 708−714.

(10) Paul, P. M.; Toma, E. S.; Breger, P.; Mullot, G.; Augé; Balcou, Ph.; Muller, H. G.; Agostini, P. Observation of a train of attosecond pulses from high harmonic generation. *Science* **2001**, *292*, 1689−1692.

(11) Li, J.; Lu, J.; Chew, A.; Han, S.; Li, J.; Wu, Y.; Wang, H.; Ghimire, S.; Chang, Z. Attosecond science based on high harmonic generation from gases and solids. *Nat. Commun.* **2020**, *11*, 2748.

(12) Ghimire, S.; Ndabashimiye, G.; DiChiara, A. D.; Sistrunk, E.; Stockman, M. I.; Agostini, P.; DiMauro, L. F.; Reis, D. A. Strong-field and attosecond physics in solids. *J. Phys. B: At. Mol. Opt. Phys.* **2014**, *47*, 204030.

(13) Luu, T. T.; Wörner, H. J. Measurement of the Berry curvature of solids using high-harmonic spectroscopy. *Nat. Commun.* **2018**, *9*, 916.

(14) Chacón, A.; Kim, D.; Zhu, W.; Kelly, S. P.; Dauphin, A.; Pisanty, E.; Maxwell, A. S.; Picón, A.; Ciappina, M. F.; Kim, D. E.; Ticknor, C.; Saxena, A.; Lewenstein, M. Circular dichroism in higher-order harmonic generation: Heralding topological phases and transitions in Chern insulators. *Phys. Rev. B* **2020**, *102*, 134115.

(15) Lou, Z.; Zheng, Y.; Liu, C.; Zeng, Z.; Li, R.; Xu, Z. Controlling of the harmonic generation induced by the Berry curvature. *Opt. Express* **2021**, *29* (23), 37809.

(16) Yoshikawa, N.; Nagai, K.; Uchida, K.; Takaguchi, Y.; Sasaki, S.; Miyata, Y.; Tanaka, K. Interband resonant high-harmonic generation by valley polarized electron-hole pairs. *Nat. Commun.* **2019**, *10*, 3709.

(17) Silva, R. E. F.; Jimenez-Galan, A.; Amorim, B.; Smirnova, O.; Ivanov, M. Topological strong-field physics on sub-laser-cycle timescale. *Nat. Photonics* **2019**, *13*, 849−854.

(18) Baykusheva, D.; Chacón, A.; Kim, D.; Kim, D. E.; Reis, D. A.; Ghimire, S. Strong-field physics in three-dimensional topological insulators. *Phys. Rev. A* **2021**, *103*, 023101.

(19) Kaneshima, K.; Shinohara, Y.; Takeuchi, K.; Ishii, N.; Imasaka, K.; Kaji, T.; Ashihara, S.; Ishikawa, K. L.; Itatani, J. Polarization-

resolved study of high harmonics from bulk semiconductors. *Phys. Rev. Lett.* **2018**, *120*, 243903.
(20) Lanin, A. A.; Stepanov, E. A.; Mitrofanov, A. V.; Sidorov-Biryukov, D. A.; Fedotov, A. B.; Zheltikov, A. M. High-order harmonic analysis of anisotropic petahertz photocurrents in solids. *Opt. Lett.* **2019**, *44*, 1888.
(21) Yu, C.; Jiang, S.; Wu, T.; Yuan, G.; Wang, Z.; Jin, C.; Lu, R. Two-dimensional imaging of energy bands from crystal orientation dependent higher-order harmonic spectra in h-BN. *Phys. Rev. B* **2018**, *98*, 085439.
(22) Morimoto, Y.; Shinohara, Y.; Tani, M.; Chen, B.-H.; Ishikawa, K. L.; Baum, P. Asymmetric single-cycle control of valence electron motion in polar chemical bonds. *Optica* **2021**, *8* (3), 382.
(23) Heide, C.; Kobayashi, Y.; Baykusheva, D. R.; Jain, D.; Sobota, J. A.; Hashimoto, M.; Kirchmann, P. S.; Oh, S.; Heinz, T. F.; Reis, D. A.; Ghimire, S. Probing topological phase transitions using high-harmonic generation. *Nat. Photonics* **2022**, *16*, 620−624.
(24) Baykusheva, D.; Chacón, A.; Lu, J.; Bailey, T. P.; Sobota, J. A.; Soifer, H.; Kirchmann, P. S.; Rotundu, C.; Uher, C.; Heinz, T. F.; Reis, D. A.; Ghimire, S. All-Optical Probe of Three-Dimensional Topological Insulators Based on High-Harmonic Generation by Circularly Polarized Laser Fields. *Nano Lett.* **2021**, *21* (21), 8970−8978.
(25) Tancogne-Dejean, D.; Mücke, O. D.; Kärtner, F. X.; Rubio, A. Ellipticity dependence of high-harmonic generation in solids originating from coupled intraband and interband dynamics. *Nat. Commun.* **2017**, *8*, 745.
(26) Sato, S. A.; Hirori, H.; Sanari, Y.; Kanemitsu, Y.; Rubio, A. High-order harmonic generation in graphene: Nonlinear coupling of intraband and interband transitions. *Phys. Rev. B* **2021**, *103*, L041408.
(27) Cha, S.; Kim, M.; Kim, Y.; Choi, S.; Kang, S.; Kim, H.; Yoon, S.; Moon, G.; Kim, T.; Lee, Y. W.; Cho, G. Y.; Park, M. J.; Kim, C.-J.; Kim, B. J.; Lee, J. D.; Jo, M.-H.; Kim, J. Gate-tunable quantum pathways of high harmonic generation in graphene. *Nat. Commun.* **2022**, *13*, 6630.
(28) Vampa, G.; McDonald, C. R.; Orlando, G.; Corkum, P. B.; Brabec, T. Semiclassical analysis of high harmonic generation in bulk crystals. *Phys. Rev. B* **2015**, *91*, 064302.
(29) Floss, I.; Lemell, C.; Wachter, G.; Smejkal, V.; Sato, S. A.; Tong, X.-M.; Yabana, K.; Burgdörfer, J. Ab initio multiscale simulation of high-order harmonic generation in solids. *Phys. Rev. A* **2018**, *97*, No. 011401(R).
(30) Du, T.-Y. Probing the dephasing time of crystals via spectral properties of high-order harmonic generation. *Phys. Rev. A* **2019**, *100*, 053401.
(31) Du, T.-Y.; Tang, D.; Bian, X.-B. Subcycle interference in high-order harmonic generation from solids. *Phys. Rev. A* **2018**, *98*, 063416.
(32) Vampa, G.; McDonald, C. R.; Orlando, G.; Klug, D. D.; Corkum, P. B.; Brabec, T. Theoretical analysis of high-harmonic generation in solids. *Phys. Rev. Lett.* **2014**, *113*, 073901.
(33) Kilen, I.; Kolesik, M.; Hader, J.; Moloney, J. V.; Huttner, U.; Hagen, M. K.; Koch, S. W. Propagation induced dephasing in semiconductor high-harmonic generation. *Phys. Rev. Lett.* **2020**, *125*, 083901.
(34) Tamaya, T.; Ishikawa, A.; Ogawa, T.; Tanaka, K. Diabatic mechanisms of higher-order harmonic generation in solid-state materials under high-intensity electric fields. *Phys. Rev. Lett.* **2016**, *116*, 016601.
(35) Sato, S. A.; McIver, J. W.; Nuske, M.; Tang, P.; Jotzu, G.; Schulte, B.; Hübener, H.; De Giovannini, U.; Mathey, L.; Sentef, M. A.; Cavalleri, A.; Rubio, A. Microscopic theory for the light-induced anomalous Hall effect in graphene. *Phys. Rev. B* **2019**, *99*, 214302.
(36) Sato, S. A.; Tang, P.; Sentef, M. A.; De Giovannini, U.; Hübener, H.; Rubio, A. Light-induced anomalous Hall effect in massless Dirac fermion systems and topological insulators with dissipation. *New J. Phys.* **2019**, *21*, 093005.
(37) Kim, Y.-S.; Lee, J.-C.; Kwon, O.; Kim, Y.-H. Protecting entanglement from decoherence using weak measurement and quantum measurement reversal. *Nat. Phys.* **2012**, *8*, 117−120.
(38) Giovannetti, V.; Lloyd, S.; Maccone, L. Advances in quantum metrology. *Nat. Photonics* **2011**, *5*, 222−229.
(39) Aeschlimann, S.; Krause, R.; Chávez-Cervantes, M.; Bromberger, H.; Jago, R.; Malić, E.; Al-Temimy, A.; Coletti, C.; Cavalleri, A.; Gierz, I. Ultrafast momentum imaging of pseudospin-flip excitations in graphene. *Phys. Rev. B* **2017**, *96*, No. 020301(R).
(40) Heide, C.; Eckstein, T.; Boolakee, T.; Gerner, C.; Weber, H. B.; Franco, I.; Hommelhoff, P. Electronic Coherence and Coherent Dephasing in the Optical Control of Electrons in Graphene. *Nano Lett.* **2021**, *21* (22), 9403−9409.
(41) Genes, C.; Berman, P. R. Atomic entanglement generation with reduced decoherence via four-wave mixing. *Phys. Rev. A* **2006**, *73*, 063828.
(42) Heide, C.; Kobayashi, Y.; Johnson, A. C.; Liu, F.; Heinz, T. F.; Reis, D. A.; Ghimire, S. Probing electron-hole coherence in strongly driven 2D materials using high-harmonic generation. *Optica* **2022**, *9* (5), 512−516.
(43) Brown, G. G.; Jiménez-Galán, A.; Silva, R. E. F.; Ivanov, M. A Real-Space Perspective on Dephasing in Solid-State High Harmonic Generation. [physics.optics] 4 Oct 2023, arXiv:2210.16889v3 (accessed 2023-12-20).
(44) Liu, C.; Zheng, Y.; Zeng, Z.; Li, R. Driving-laser ellipticity dependence of high-order harmonic generation in graphene. *Phys. Rev. A* **2018**, *97*, 063412.
(45) Boolakee, T.; Heide, C.; Garzon-Ramirez, A.; Weber, H. B.; Franco, I.; Hommelhoff, P. Light-field control of real and virtual charge carriers. *Nature* **2022**, *605*, 251−255.
(46) Zhu, T.; Antezza, M.; Wang, J.-S. Dynamical polarizability of graphene with spatial dispersion. *Phys. Rev. B* **2021**, *103*, 125421.
(47) Feng, Y.; Shi, S.; Li, J.; Ren, Y.; Zhang, X.; Chen, J.; Du, H. Semiclassical analysis of ellipticity dependence of harmonic yield in graphene. *Phys. Rev. A* **2021**, *104*, 043525.

https://doi.org/10.1021/acs.nanolett.3c04278
Nano Lett. 2024, 24, 1277−1283